Collective spin in twisted bilayer materials

Zhigang Song,[1] Jingshan Qi,[2,*] Olivia Liebman,[3] and Prineha Narang[3,†]
[1]*John A. Paulson School of Engineering and Applied Sciences, Harvard University, Cambridge, Massachusetts 02138, USA*
[2]*School of Science, Tianjin University of Technology, Tianjin 300384, China*
[3]*College of Letters and Sciences, University of California Los Angeles, Los Angeles, California 90095, USA*

(Received 17 July 2023; revised 29 February 2024; accepted 3 June 2024; published 1 July 2024)

Twisting has been demonstrated as a technique for creating strongly correlated effects in two-dimensional bilayered materials and can tunably generate nontrivial topological properties, magnetism, and superconductivity. Magnetism is particularly significant, as it can both compete with superconductivity and lead to the emergence of nontrivial topological states. Due to the technique challenges in theoretical methods without input parameters, theorical studies on twisted materials beyond twisted bilayer graphene are rarely reported. Thus, first-principles studies on a wide range of materials are expected in both fields of fundamental physics and materials science. By using self-developed large-scale density functional theory calculations uniquely capable of simulating twisted systems, we found the ferromagnetism arising due to spin splitting in different twisted bilayer systems across various two-dimensional materials, such as twisted bilayer h-BN, $2H-MoTe_2$, PbS, and $2H-NbSe_2$. The spin splitting itself is induced by the enhanced ratio of the exchange interaction to band dispersion near the Fermi level. An important discovery in this paper is that, in some nonmagnetic metallic bilayers, e.g., $2H-NbSe_2$ and $1T-MoS_2$, twisting transforms a nonmagnetic state into a collective ferromagnetic state even without any doping.

DOI: 10.1103/PhysRevB.110.024401

I. INTRODUCTION

Moiré superlattices formed by twisted bilayer graphene (TBG) have attracted significant interest due to their intriguing strongly correlated physics when doped at low temperature [1,2]. At each integer electron or hole filling, TBG exhibits strongly correlated Chern insulator behavior. When slightly deviated away from integer filling for hole-type carriers, superconductivity has been observed at the magic angle [2–8]. Studying superconductivity at the magic angle demands an understanding of the transition from magnetic to nonmagnetic states [4,7,9–21]. Magnetization is a prerequisite for the presence of correlated Chern insulators and other topological and magnetic phenomena [7,16,22–27]. As one of basic physical properties, the magnetism in TBG has rarely been studied with first-principles methods. Moreover, in other twisted bilayer materials, e.g., twisted bilayer $2H-MoTe_2$, ferromagnetism has been observed when it is quarter-filled with electrons [28], suggesting that magnetization is a general phenomenon in twisted materials with flat bands. Due to the technique challenges in theoretical methods without input parameters, theoretical studies on twisted materials beyond TBG are few. Thus, first-principles (which is parameter free) studies on a wide range of materials are expected in both fields of fundamental physics and materials science.

Despite numerous experimental observations in TBG [29–31], theoretical predictions on the origin of magnetism have not been in alignment with experimental data. One argument for the origin of magnetism in TBG comes from its nontrivial topology [32–35]. Thus, in previous reports, ferromagnetism was proposed as orbital ferromagnetism arising from the Berry curvature and induced nonlocal current [29,30,34,36–39]. Orbital ferromagnetism [40] has attracted perhaps excessive attention from experimentalists seeking to answer the question of magnetism in twisted bilayer systems. However, several puzzles arise when experimental researchers attempt to find evidence for orbital ferromagnetism. For example, Berry curvature and nonlocal current in two-dimensional materials can induce an orbital moment that is only vertical to the material plane, but experimental measurements show that the Hall effect has a large response to an in-plane magnetic field [30]. In addition, the measured magnetic moment ($\sim 2\,\mu_B$) [40] is always less than the theoretically predicted orbital moment ($5-10\,\mu_B$) [33]. Although alignment with h-BN is necessary to induce a small band gap and large valley-contrast Berry curvature in TBG, ferromagnetism has also been observed without h-BN alignment [30]. Even for a large twist angle of 1.6°, ferromagnetism was also observed in experiments [41]. Additionally, isospin behaviors are also thought to be closely related to magnetic properties in TBG and so on [31]. These puzzles suggest that the origin of magnetism may not or at least may not solely come from orbital magnetic moments and that electron spin may be another crucial factor.

In theory, different possible magnetic ground states have been proposed even for the same materials, including the well-studied TBG [4,10,12,18,26,34,42–68]. This can lead to inconsistencies or even incorrect predictions due to various

*Contact author: qijingshan@email.tjut.edu.cn
†Contact author: prineha@ucla.edu

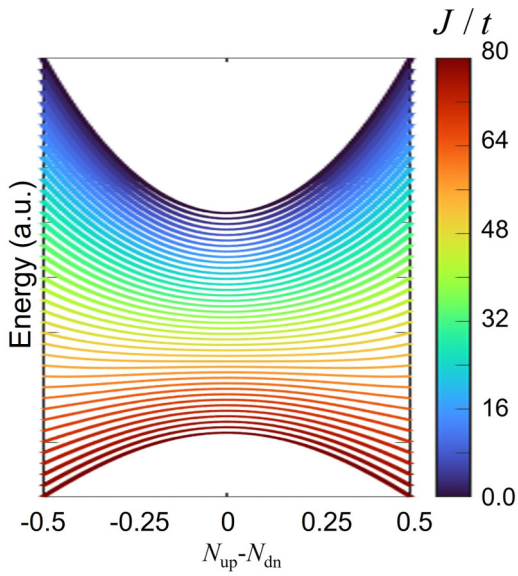

FIG. 1. Energy as a function of occupation difference between the spin-up and spin-down bands ($N_{up} - N_{dn}$). The band is half occupied. Color varying from blue and red corresponds to the increase of the ratio J and t. t is set as 1.

approximations and lack of specific material parameters. As a first-principles method, density functional theory (DFT) has the potential to shed light on these puzzles, as demonstrated by its years of successful computational predictions [69]. Due to the challenge of extremely large supercell size, the spin-polarized electronic structure study of TBG has been largely unattainable until now. Through use of our self-developed code (PWMAT) [70], we are uniquely capable of efficiently simulating large supercells containing 10 000 atoms or more. We have confirmed the accuracy of this method in previous work by comparing it with experiments [71–73]. Our calculations use a single-ζ atomic basis set, the PBE exchange-correlation functional, and Fritz-Haber-Institute (FHI) pseudopotential, which is a norm-conserving pseudopotential with a single projector for each angular momentum and without semicore states [74]. To include the interlayer molecular interaction, we applied the DFT-D2 method [75] and relaxed the atomic positions in the twisted structures until the force on each atom was $< 0.03\,\text{eV/Å}$. The lattice is fixed according to the equilibrium lattice of corresponding monolayer materials. We used a $2 \times 2 \times 1$ k mesh when the twisted angle was $< 1.65^\circ$ and set the temperature in Fermi smearing as 3 K. Here, we use large-scale spin-polarized DFT calculations to compute the spin response to different doping in different twisted layers with small twist angles. Spin-orbit coupling is neglected. Usually, a linear spin-polarized approximation is good enough to calculate spin polarization in quality, although spin-orbit coupling will quantitatively lead to an error. Our results show that localization-induced spin splitting is a universal mechanism for the physical origin of magnetism in twisted layers with a small twist angle.

II. *t-J* MODEL

To obtain the main physics for our limited DFT calculations in the next part, we start from a toy t-J model, which describes the spin splitting upon doping:

$$H = \sum_{ij} t_{ij} c_i^\dagger c_j + \text{H.c.} + \sum_{ij} J_{ij} S_i^z S_j^z, \tag{1}$$

where t_{ij} represents the hopping integral between orbitals on different lattice sites i and j, J_{ij} is the effective exchange interaction, $c_j^\dagger$ (c_i) creates (annihilates) an electron on site j (i), and S^z is the typical spin-projection operator in the z direction. Under decreasing twist angle, the bands tend to flatten out as the lattice parameter increases. This band flattening implies large electron effective mass, a quenching of the electronic hopping kinetic energy, and the extended electronic states to become localized. As the twist angle decreases, both t and J decrease. Although the exact functional dependence of t and J on the twist angle is unknown, the ratio of J/t always increases with respect to the decreasing twisting angle [76]. We solve the above model Hamiltonian using a two-dimensional toy model of one orbital on a square lattice. The ground states are obtained by minimizing the energy by varying the occupation of spin-up N_{up} and spin-down N_{dn} bands, while we keep a total occupation, which corresponds to a certain doping. The energy landscape of the model in the

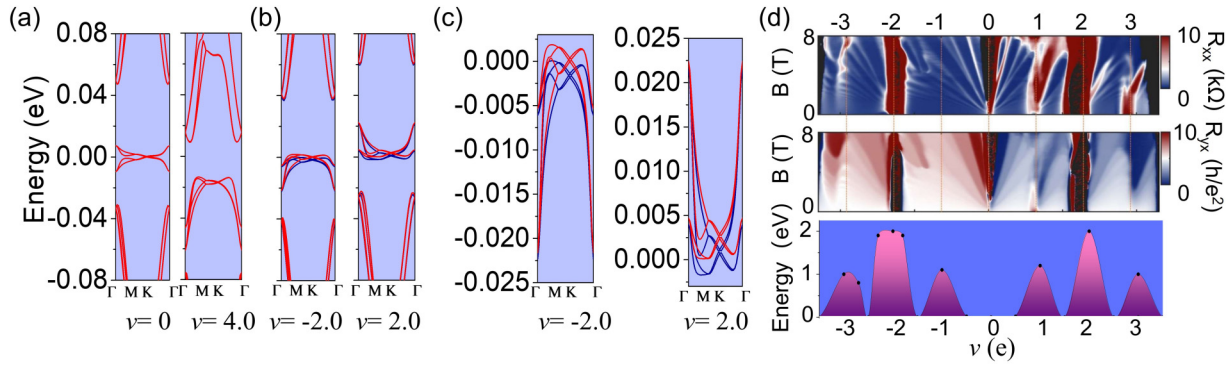

FIG. 2. (a) and (b) Spin-polarized band structures with different doping (υ) in a supercell for twist angle of 1.47°. The Fermi level is set as 0. (c) Zoom in of (b). Red and blue are spin-up and spin-down channels, respectively. (d) Comparison between the experimental phase diagram (figure from Ref. [14]) and calculated spin splitting upon doping.

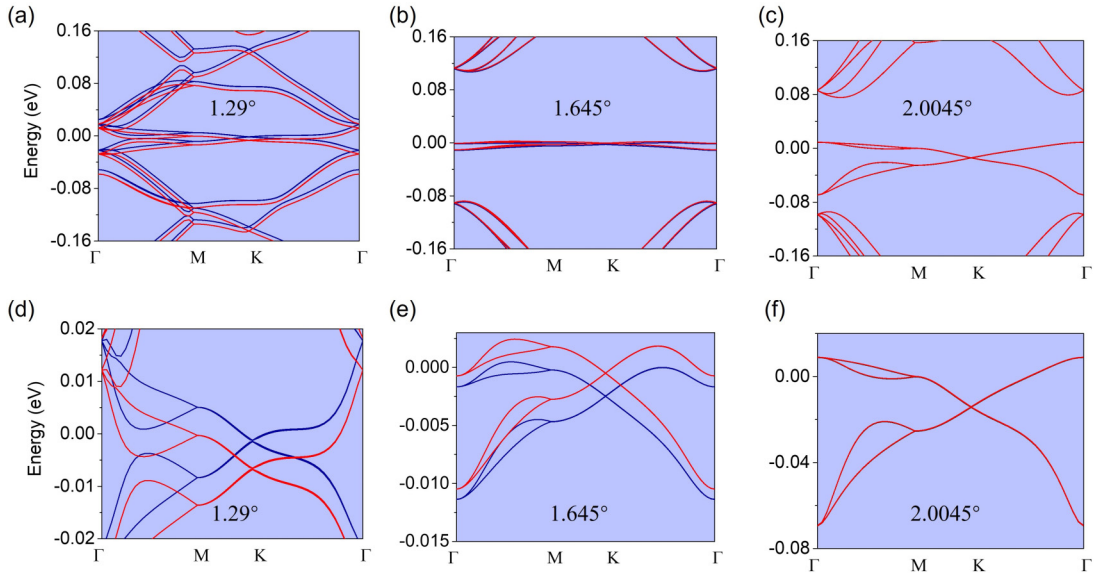

FIG. 3. (a)–(c) Spin-polarized band structures under different twist angles. The filling factor is $\nu = 2$. (d)–(f) Zoom in on (a)–(c) near the Fermi level. Red and blue are spin-up and spin-down channels, respectively.

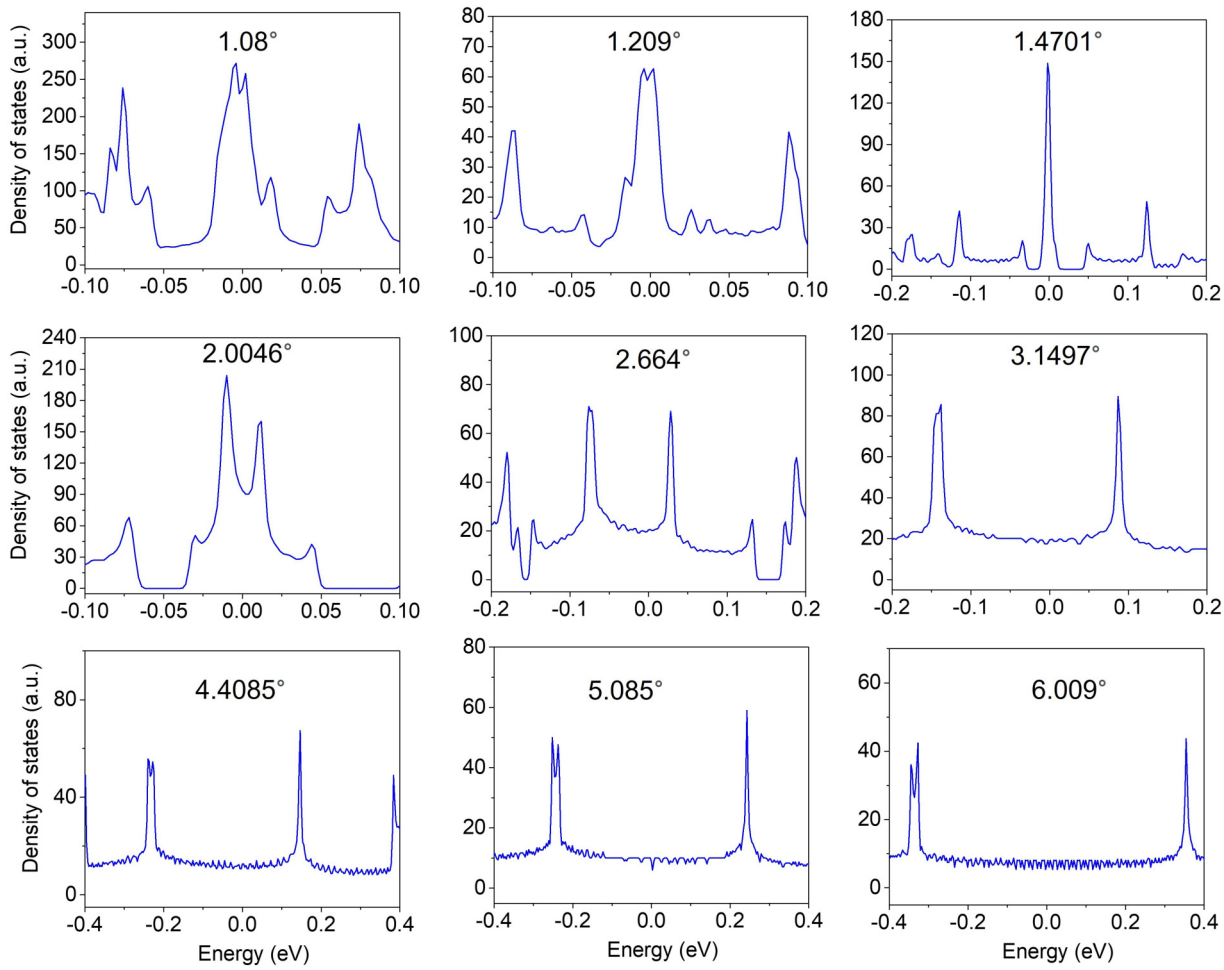

FIG. 4. Density functional theory (DFT) calculated density of states in twisted bilayer graphene with different twist angles. No doping was applied. Spin polarization is turned off. A smearing of 6 meV is applied.

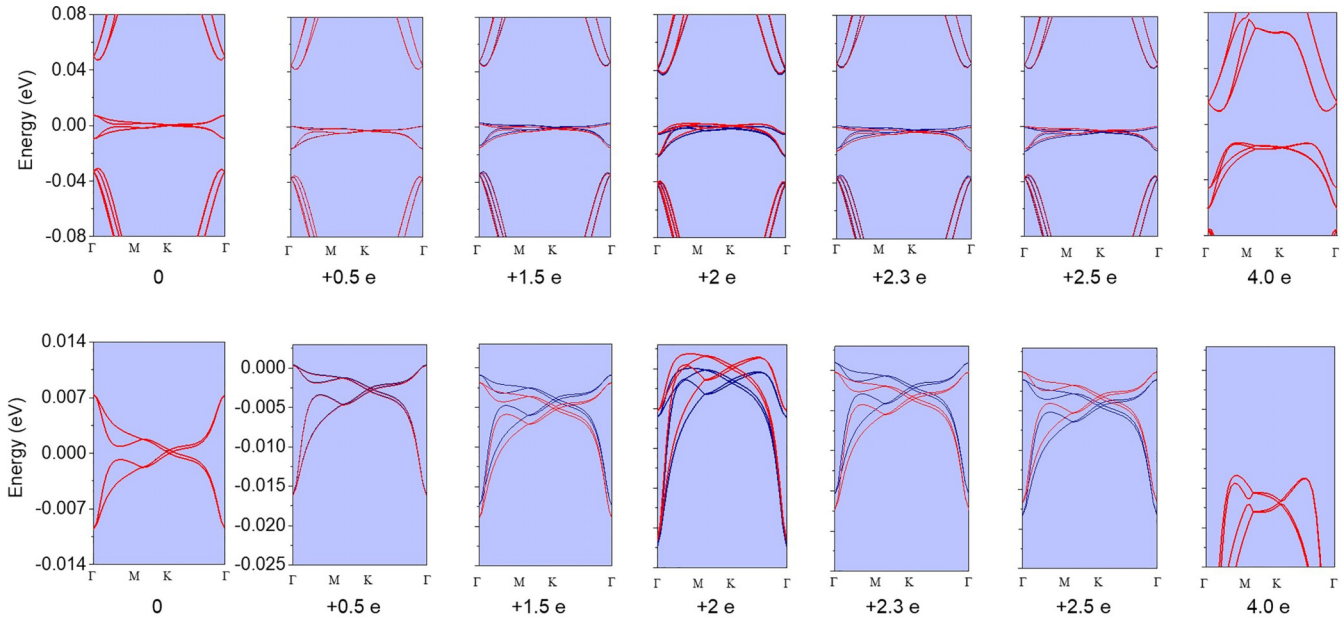

FIG. 5. Spin-polarized band structures of twisted bilayer graphene with different filling factor. Lower row is the corresponding zoom in the upper row near the Fermi level.

case of half occupation is shown in Fig. 1. If the ratio (J/t) of exchange interaction to band dispersion is small, doping does not induce spin polarization. On the other hand, when J/t is large, doping induces nonzero magnetization to a lower total free energy.

III. ELECTRONIC STRUCTURE OF TBG

Next, we perform spin-polarized DFT calculations of TBG, which has received extensive experimental interest. The largest system being calculated consists of 9076 atoms. In the absence of doping, the spin-up and spin-down bands are degenerate for any twist angle. However, when the twist angle is reduced $< 1.65°$, the spin splitting jumps to a nonzero value upon doping with two electrons. This leads to a breaking of the degeneracy of the spin-up and spin-down bands, as in Figs. 2(a)–2(c) and 3 for twist angles of 1.29°, 1.47°, and 1.65°. As the Fermi level crosses the bands, the number of electrons with spin-up and spin-down is no longer equal, resulting in a net spin moment. Despite the angle of 1.65° being slightly larger than the common magic angle of 1.08° in strongly correlated physics, ferromagnetism was observed experimentally at this twist angle [41].

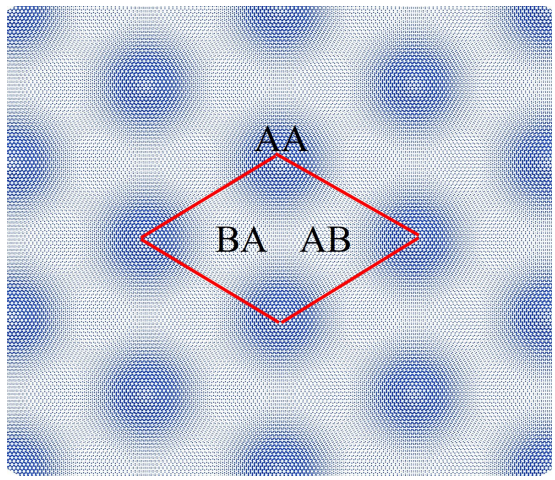

FIG. 6. Spin density in the range of ±5 meV around the Fermi level under a twist angle of 1.47°. The red frame implies a moiré unit cell.

To investigate the effect of doping on spin splitting and band dispersion, we focused on a twist angle of 1.47°. Figure 2(d) shows the spin splitting for different filling factors υ. Without any doping, the conduction and valence bands look similar aside from the slight particle hole asymmetry. This result is in good accordance with previous results obtained by different methods [77–79]. The corresponding density of states are shown in Fig. 4. Figure 2(d) shows that when the number of doped electrons is < 0.5 e/supercell, the spin splitting remains at zero. However, as the number of doped electrons increases, the spin splitting also increases and reaches a maximum average spin splitting at a doped electron number of 2 ($\upsilon = 2$). After that, the spin splitting begins to decrease with further doping. At the filling factor $\upsilon = \pm 2$, the maximum spin splitting is ~ 2.5 meV, resulting in a maximum spin magnetic moment of $1.6\,\mu_B$ in each moiré unit cell. Compared with the spin nonpolarized state, the energy decreases by 6 meV after including the spin polarization. At the filling factors $\upsilon = 1$ or 3, the spin magnetic moment is as large as $0.8\,\mu_B$ in one moiré unit cell. When the doped electron number > 3.5, the spin splitting becomes zero again. When the number of doped electrons reaches 4, the Fermi level enters the band gap, tuning the material into a band insulator with zero spin moment and spin splitting. The band structures with different filling factors are shown in Fig. 5. Our results suggest that the doping-induced spin splitting is likely

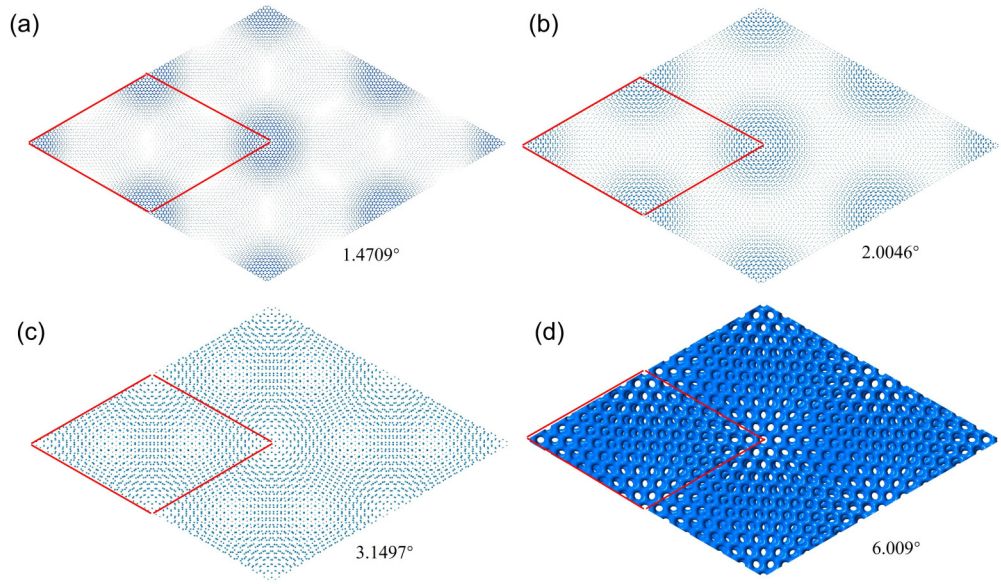

FIG. 7. (a)–(d) Charge density of twisted bilayer graphene in the range from ±5 meV near the Fermi level under different twist angles, given above. Red frames imply the moiré unit cells. In (a), the charge density is approximately equal to spin density. In (b)–(d), there is no spin polarization.

to be the primary reason for the magnetic properties of the system, with the magnetic moment ($\sim 1.6\,\mu_B$) caused by spin polarization being closer to the experimental measurements ($\sim 2\,\mu_B$) in the case of $v = 2$. In DFT calculations, we cannot include spin fluctuations, so we failed to capture the Pomeranchuk effect at $v = -1$, as has been seen in experiments [31,80].

A spin density near the Fermi level is shown in Fig. 6. As the twist angle decreases, the electron density becomes more localized. At the twist angle of 1.47°, the electron density is almost exclusively localized in a zone of AA stacking, which is consistent with previous experimental findings [41]. The charge pattern forms a ring with a small pseudohole at the center, where the electron density is small but not zero. The average radius of the ring is ~ 2.0 nm, indicating that the spin magnetic moment is not localized at the atomic scale. Instead, it is a collective contribution from several hundred carbon atoms and exhibits a periodic pattern. This is in contrast with common magnetic materials, such as iron, manganese, and chromium [70], where one spin is typically localized on a single atom [69]. In addition, our DFT calculations show that the spin density mostly resides in the region with remarkable in-plane relaxation, indicating a spin-lattice coupling (see Figs. 7 and 8).

As discussed above, spin splitting is correlated with electron occupation on flat bands near the Fermi level since the electron occupation and spin splitting change coherently where, if one of them is changed, the phase transition can be driven. In our calculations, we include the effect of temperature in the Fermi smearing, which shows that when the temperature is > 10 K, the spin splitting induced by doping disappears. Superconductivity is not yet captured in DFT calculations due to the absence of electron-electron interaction, so the phase transition to superconductivity was not captured in the present calculations. With the aid of experiments, we tried to include the electron and hole occupation effects. Both the calculated spin splitting and the experimental anomalous Hall effect imply broken time-reversal symmetry, while the peak positions in doping should be the same. Indeed, the calculated phase diagram of the twisted bilayer is in good accordance with the summary from experimental measurements, as shown in Fig. 2(d).

IV. SPIN POLARIZATION IN DIFFERENT TWISTED BILAYER MATERIALS

Guided by the toy model, we also used DFT calculations to investigate the magnetization in typical twisted bilayers of h-BN, $2H - MoTe_2$, PbS, and $2H - NbSe_2$. The results are shown in Figs. 9 and 10. At larger twist angle, the moiré period is short, and wave functions are nonlocal. Thus, the spin splitting is zero. The spin splitting usually increases and then decreases as the twist angle decreases. The twist angle which yields the spin splitting is material dependent, as shown in Fig. 9, e.g., in TBG, the spin splitting peaks $\sim 1.47°$. In twisted bilayer h-BN, spin splitting decreases with decreasing twist angle. In an example of twist angle of 2.0046° for h-BN, the spin splitting is 13.5 meV (details in Fig. 11). Another interesting discovery is that the spin-polarized bands are twofold degenerate due to the $U_v(1)$ valley symmetry emergent in the small angle limit [81]. As shown in Fig. 12, the wave functions are localized in real space. If the twist angle is small enough (such as 2.0046° and 1.6459°), it leads to a magnetic moment of $2\,\mu_B$, when two electrons are doped. The total spin will be 1 rather than $\frac{1}{2}$, and it will split into $S_z = 0, \pm 1$ under a vertical magnetic field. This finding indicates that the electronic structures are like the states of nitrogen-vacancy centers in diamond [82–84], so the twisted h-BN with proper doping could have possible application as a quantum bit. In twisted bilayer PbS, the largest spin splitting

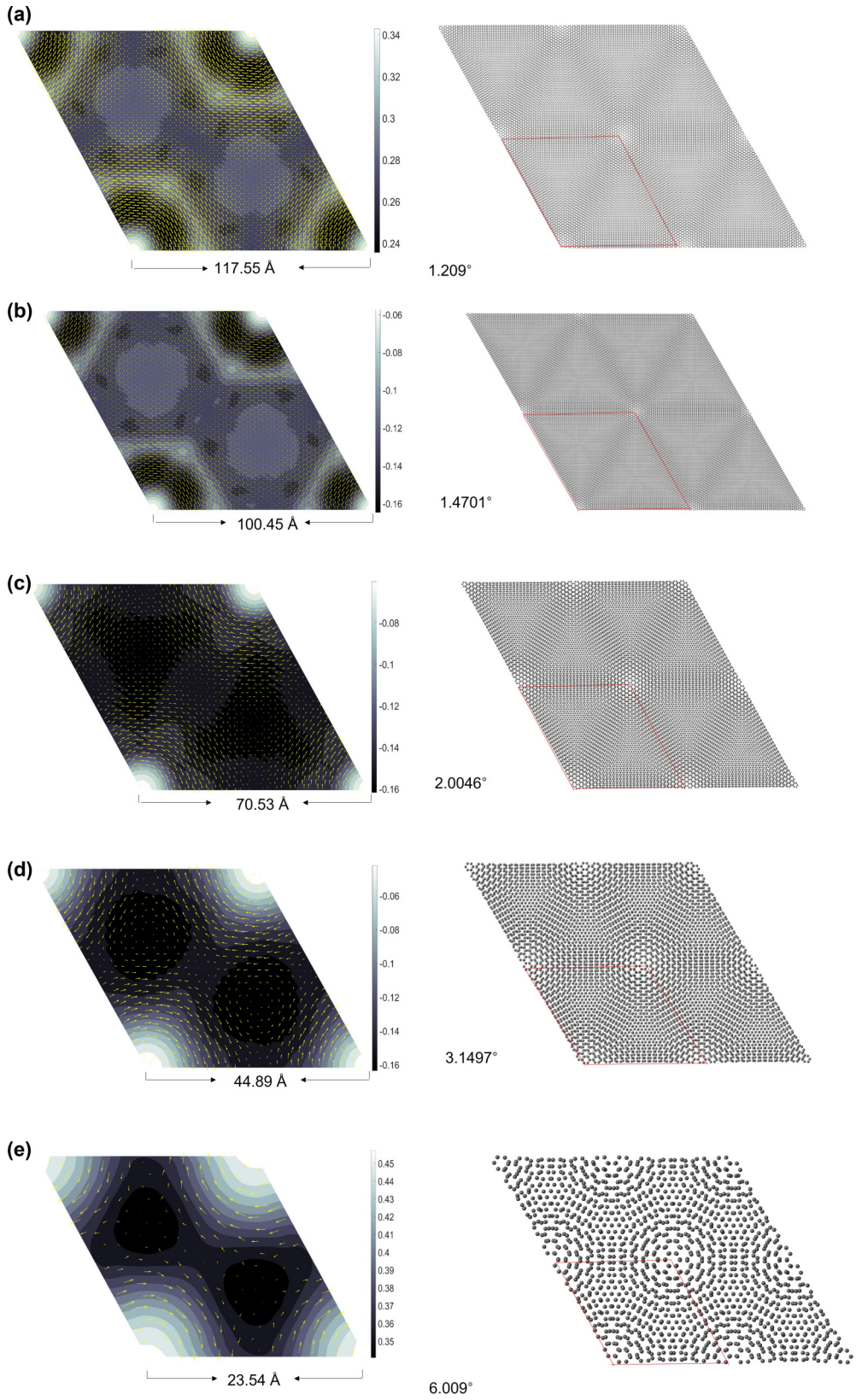

FIG. 8. Density functional theory (DFT) relaxed structures of twisted bilayer graphene in the range of small twist angles. (a)–(e) Twist angles are 1.2029°, 1.4701°, 2.0046°, 3.1497°, and 6.009°. Left panels are maps of atomic displacement in a moiré unit cell, and right panels are the atomic structure of relaxed structure in a $2 \times 2 \times 1$ moiré cell. Red frames represent moiré unit cells.

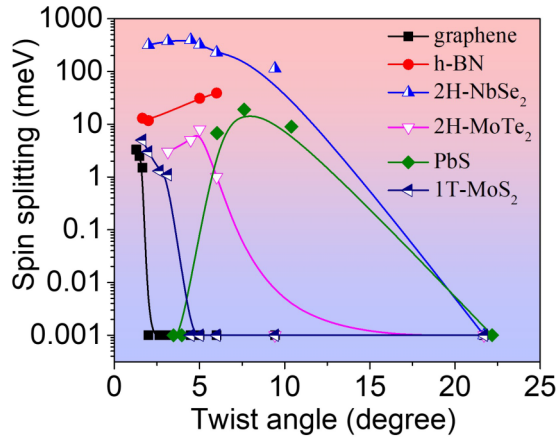

FIG. 9. Spin splitting as a function of twist angle for different materials. A small shift of 0.001 meV is applied for plotting.

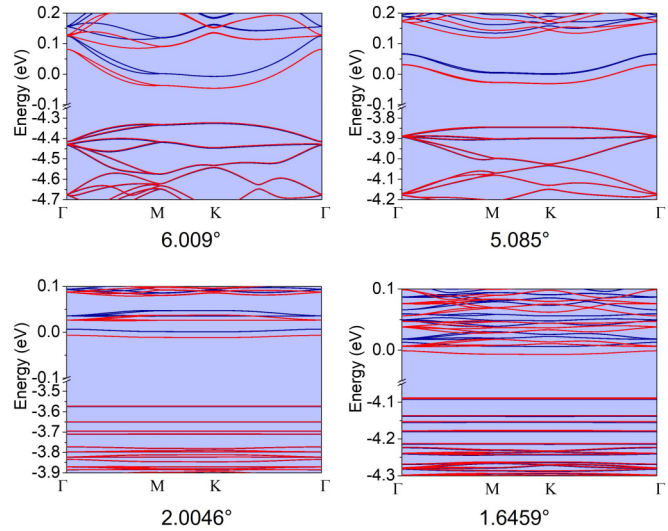

FIG. 11. Spin-polarized band structures of twisted bilayer *h*-BN under different twist angles. The filling factor is $\upsilon = 2$.

occurs roughly at a twist angle of 7.8° (details in Fig. 13). In a typical twist angle of 6.025°, the spin splitting is 7.1 meV, and the magnetic moment is $2\,\mu_B$ when two electrons are doped into the twisted bilayer PbS [71]. The spin density is mainly localized at AA stacking zones, as shown in Fig. 14. In electron-doped twisted bilayer $2H - MoTe_2$, the peak of spin splitting occurs at 5.085°. Band structures under small twist angles of 4.4085° and 5.085° and spin density is shown in Figs. 15 and 16, respectively. In experiments, ferromagnetism has been observed in twisted bilayer $MoTe_2$ with a twist angle $\sim 4°$ when doped.

Doping is not necessary in a metallic twisted bilayer. Here, we consider the effects of twist on spin polarization of undoped bilayer $2H - NbSe_2$, which is a nonmagnetic metal. The temperature is set at 100 K. In the large twisted angle $> 9.43°$, there is no spin polarization, yet as the twist angle decreases, the spin splitting increases. When the twist angle decreases to 4.4085°, spin splitting can be as large as 0.4 eV. The spin-polarized state is 48 meV lower than the spin-nonpolarized state. The spin-polarized band structure and spin density are shown in Figs. 9(d), 17, and 18. The spin moment in a moiré supercell is $\sim 109\,\mu_B$, a very large value compared with doped bilayer graphene. When the twist angle decreases to 3.1497°, the spin moment increases to $\sim 390\,\mu_B$. Similar phenomena have also observed in twisted $1T - MoS_2$, and the twist-dependent spin polarization is shown in Fig. 19. The magnetism comes from the local atomic magnetic moment. The interlayer twisting does not fundamentally change the

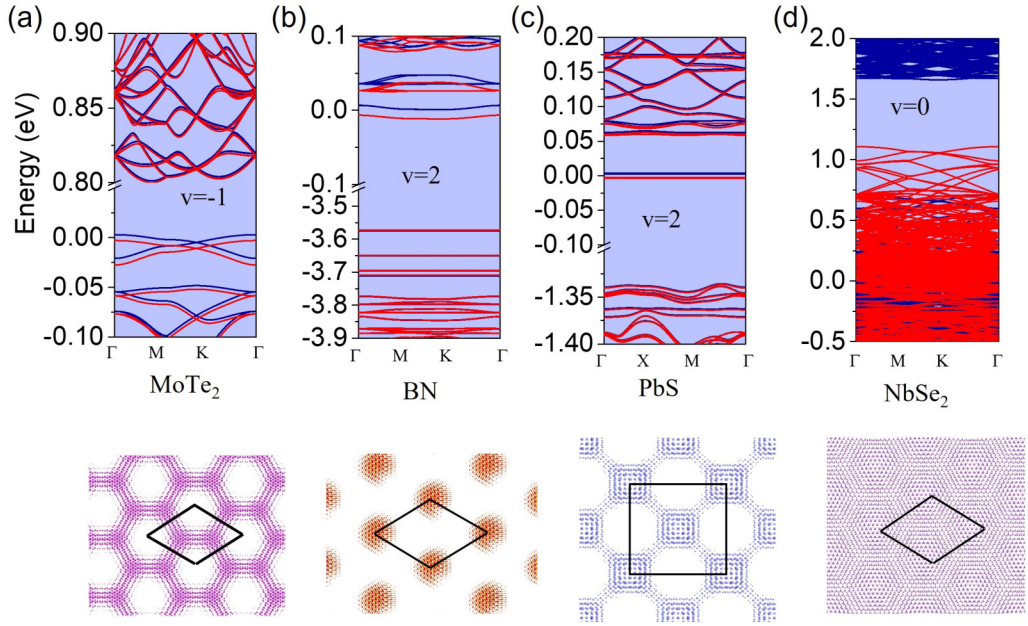

FIG. 10. Band structures (upper panels) and corresponding spin density near the Fermi level (lower panels). (a) Bilayer $2H - MoTe_2$ twisted by 4.4085°. (b) Bilayer *h*-BN twisted by 2.0046°. (c) Bilayer PbS twisted by 6.0256°. (d) Bilayer $2H - NbSe_2$ twisted by 4.4085°. The Fermi level is set as 0. Lower panels are corresponding spin density near the Fermi level.

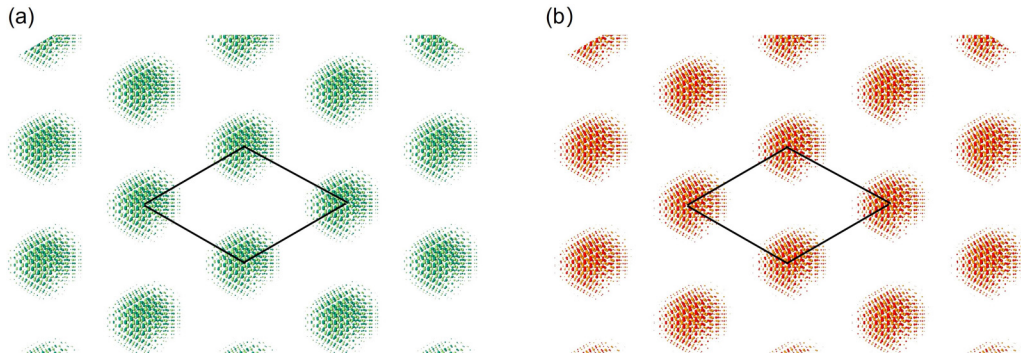

FIG. 12. Spin-polarized wave functions of twisted bilayer *h*-BN. The filling factor is $\upsilon = 2$. Red and orange are Bloch wave functions of two degenerate bands below the Fermi level. Twist angle here is 2.0045°.

local atomic structure and bonding but rather transforms a nonmagnetic material into a magnetic material by changing the electron correlation. This is undoubtedly an important previously undiscovered characteristic, which expands the research fields of twistronics.

Spin magnetism here is of Stoner type rather than Heisenberg magnetism. In a Heisenberg magnet, a magnetic moment has a constant magnitude localized on an atom and can orientate in any direction. In a Stoner magnet, the magnitude of magnetic moments varies upon electron excitation [85]. In fact, Stoner ferromagnetism stems from strongly correlated phenomena, and the derivation from the interacting Hamiltonian is seen in the Appendixes. DFT includes the electron-electron interaction in the mean-field method. The exchange interaction part is included by exchange-correlated functional. Thus, DFT calculations of magnetism here stem from the correlated physics.

In conclusion, we have performed large-scale, spin-polarized DFT calculations to study the magnetism in a host of different twisted bilayer materials. We propose the underlying source of ferromagnetism arises from the relationship

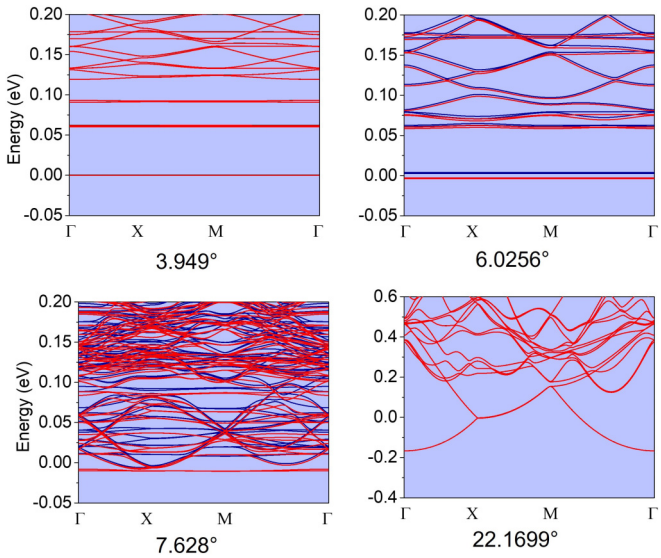

FIG. 13. Spin-polarized band structures of bilayer PbS under different twist angles. The filling factor is $\upsilon = 2$.

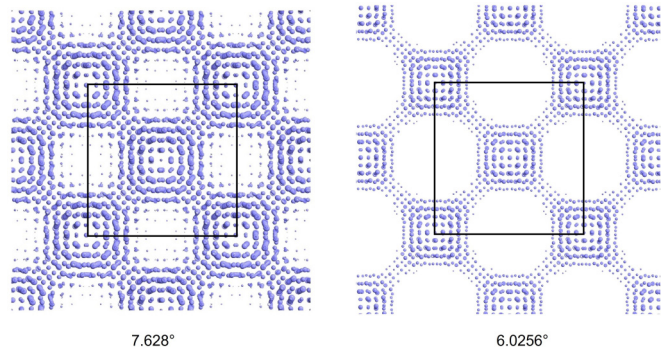

FIG. 14. Spin density of twisted bilayer PbS. The filling factor is $\upsilon = 2$. The charge density is cut off in the range from −0.2 to 0 eV.

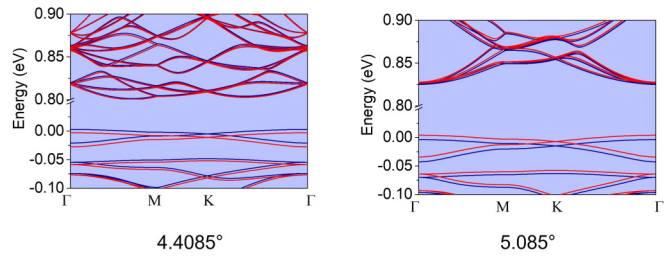

FIG. 15. Spin-polarized band structures of twisted bilayer $2H - MoTe_2$ under different twist angles. The filling factor is $\upsilon = -1$.

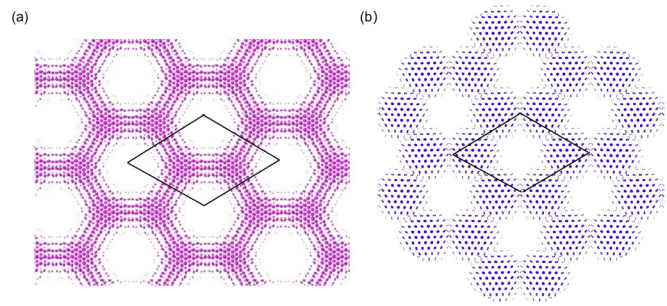

FIG. 16. Spin density of twisted bilayer $2H - MoTe_2$. (a) The filling factor is $\upsilon = -1$. The charge density is cut off in the range from 0 to 0.1 eV. (b) The filling factor is $\upsilon = 1$. The charge density is cut off in the range from −0.2 to 0 eV. Twist angle is 4.4085°.

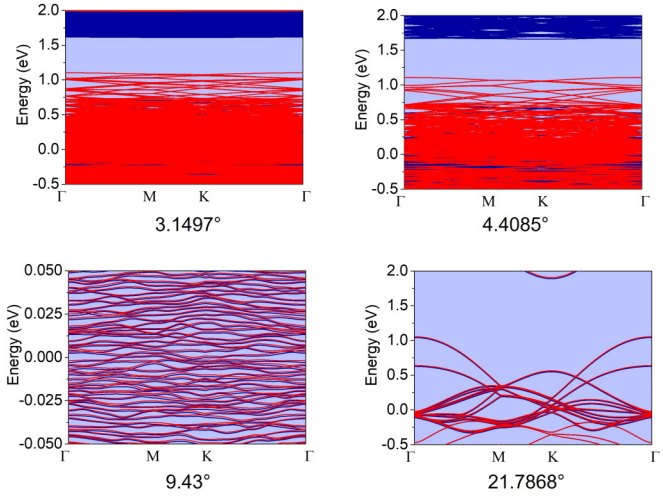

FIG. 17. Spin-polarized band structures of twisted bilayer $2H-NbSe_2$ under different twist angles. The filling factor is $v=0$. No doping is applied.

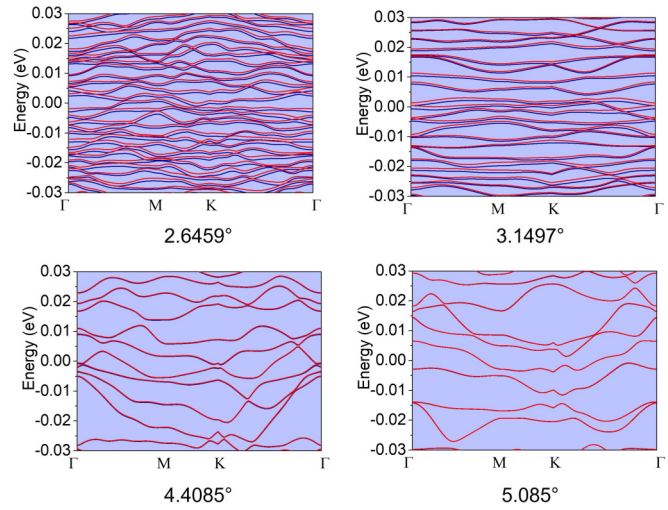

FIG. 19. Spin-polarized band structures of twisted bilayer $1T-MoS_2$ under different twist angles. The filling factor is $v=0$. No doping is applied.

between twist angle and induced spin-splitting effects such that, at specific twist angles, the spins nonlocally and collectively polarize. We assert this fundamental origin of magnetism in these structures is in better agreement with experimental results, e.g., the case of TBG and its cascade of phase transitions upon doping. Our calculations show that the twisted-induced magnetism is not unique to TBG but can be observed in other twisted systems as well. To our surprise, in some nonmagnetic metallic bilayers, such as bilayer $2H-NbSe_2$ and $1T-MoS_2$, twisting can transform a nonmagnetic state into a ferromagnetic state without doping. This is the most important discovery in this paper. We finish by suggesting potential application of the localized spin states for use in quantum simulators.

ACKNOWLEDGMENTS

This paper is partially supported by the Quantum Science Center, a National Quantum Information Science Research Center of the U.S. Department of Energy. P.N. gratefully acknowledges support from the Gordon and Betty Moore Foundation Grant No. 8048 and from the John Simon Guggenheim Memorial Foundation (Guggenheim Fellowship). We thank Y. Wang from the Department of Physics at Harvard University for fruitful discussions.

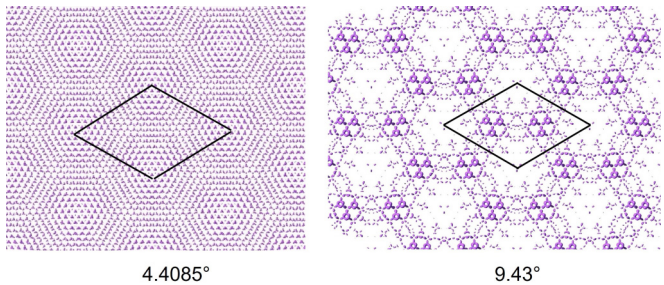

FIG. 18. Spin density of twisted bilayer $2H-NbSe_2$. The spin density is cut off in the range from -0.3 to 0.3 eV. No doping is applied. The spin density under twist angle of 21.78° is zero.

APPENDIX A: DERIVATION OF STONER MODEL FROM INTERACTING HAMILTONIAN

According to Bloch theory including interaction, a general Hamiltonian is as follows:

$$H=\sum_{\sigma k}\varepsilon_k a_k^\dagger a_k+\sum_q\frac{U(q)}{V}\sum_{\sigma k\sigma' k'}a_{\sigma k+q}^\dagger a_{\sigma' k'-q}^\dagger a_{\sigma' k'}a_{\sigma k},\tag{A1}$$

where V is the volume, $U(q)$ is momentum-resolved Coulomb interaction, q and k represent momentum vectors, and σ and σ' represent a spin with a twofold degree of freedom. In a special case, $U(q)=U_0$ is a constant. We denote $U_0/V=J$. Equation (A1) can be transfer into Eq. (1) by Fourier transformation. The only difference is a constant:

$$H=\sum\nolimits_{<ij>}t_{ij}c_i^\dagger c_j+\text{H.c.}+\sum\nolimits_{<ij>}J_{ij}\left(S_i^zS_j^z-\frac{n_in_j}{4}\right).\tag{A2}$$

The Hamiltonian in Eq. (A1) can be decomposed into noninteracting part H_0 and interacting part H_c. We now solve this Hamiltonian in the method of the variational process. The Slater determinants of single-particle states ($|\varphi_0\rangle$) of the noninteracting part H_0 work as the reference states. This is equivalent to the Hartree-Fock decoupling. The energy of the interaction part is

$$\langle\varphi_0|H_c|\varphi_0\rangle=\sum_q\frac{U(q)}{V}\sum_{\sigma k\sigma' k'}\langle\varphi_0|a_{\sigma k+q}^\dagger a_{\sigma' k'-q}^\dagger a_{\sigma' k'}a_{\sigma k}|\varphi_0\rangle,\tag{A3}$$

where $|\varphi_0\rangle$ is a Fermi sea, where all states below the Fermi level are occupied, and all states above the Fermi level are unoccupied. The expectation value under the summary is nonzero only if the creation and annihilation operators are

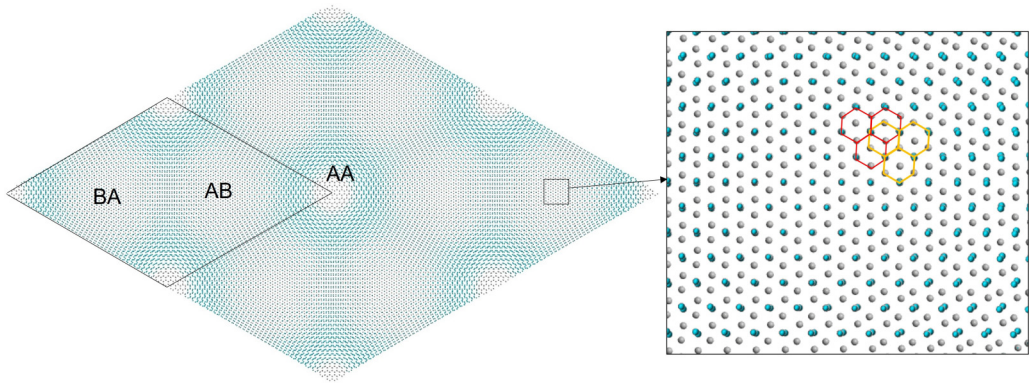

FIG. 20. Spin density in the range of ±5 meV around the Fermi level under a twist angle of 1.47°. The black frame implies a moiré unit cell. Insert is zoom in of AB stacking part. AA represents that the atoms at an upper layer stack directly on the top of atoms at a lower layer. AB (BA) represents that the atoms at an upper (lower) layer stack on (below) the centers of atom hexagons of a lower (upper) layer. Red and orange outline the atoms at upper and lower layers.

paired, i.e., (a) $k+q=k$ and $k'-q=k'$ or (b) $k+q=k'$ and $\sigma=\sigma'$. In case (a),

$$\langle\varphi_0|H_c|\varphi_0\rangle=\frac{U(0)}{V}\langle\varphi_0|\left(\sum_{\sigma k}a^\dagger_{\sigma k}a_{\sigma k}\right)^2|\varphi_0\rangle=N^2\frac{U(0)}{V}. \tag{A4}$$

This term is a spin-independent constant, and it only contributes to an energy shift. It will not induce spin polarization, and thus, we neglect this term. In case (b),

$$\langle\varphi_0|H_c|\varphi_0\rangle=-\sum_{\sigma k,k'\neq k}\frac{U(k'-k)}{V}\langle\varphi_0|a^\dagger_{\sigma k'}a_{\sigma k'}a^\dagger_{\sigma k}a_{\sigma k}|\varphi_0\rangle. \tag{A5}$$

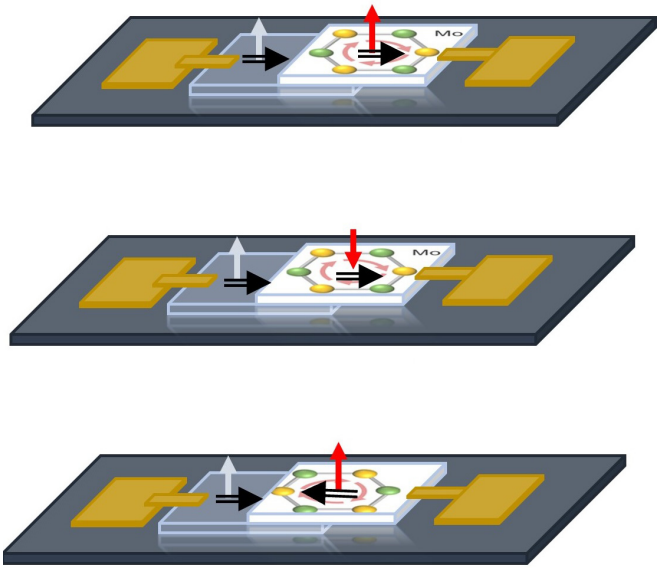

FIG. 21. Illustration of proposed experiments. In a device, the left part of the heterostructure is twisted bilayer graphene, and the right part is Mn-doped MoS_2. Arrows represent the applied magnetic field. In-plane double arrows present the valley pseudospin.

The system energy is

$$E=\sum_{\sigma k}\varepsilon_{\sigma k}n_{\sigma k}-\sum_{\sigma k,k'\neq k}\frac{U(k'-k)}{V}n_{\sigma k'}n_{\sigma k} \tag{A6}$$

without electron-phonon coupling, $U(k'-k)$ is repulsive, and it is positive. We see that the energy decreases when electrons have parallel spins, resulting in a ferromagnetic exchange interaction between the electrons.

As in Eq. (A2), we assume $U(k'-k)/V=J$ is a constant. Equation (A6) is reduced into an effective Stoner model:

$$E=\sum_{\sigma k}\varepsilon_{\sigma k}n_{\sigma k}-J(N^2_\uparrow+N^2_\downarrow). \tag{A7}$$

In fact, DFT includes the electron-electron interaction in the mean-field method. The exchange interaction part is included by exchange-correlated functional. Here, we adopted the PBE method. Thus, DFT calculations of magnetism are possibly stemmed from the correlated effect in physics. In our calculations of TBG, the basic physics can be well captured. As shown in Fig. 20, the zoom-in of spin density shows the spin-polarized states are layer-locked in TBG. The spin-polarized states in the AB stacking zone prefer to be distributed at the A sublattice of the top layer and the B sublattice of the bottom layer. The spin-polarized states in the BA stacking zone are distributed at the opposite sublattice of the opposite layer. The spin polarization here is in accordance with the spin magnetism proposed in some of the previous experiments.

APPENDIX B: PROPOSED EXPERIMENT TO DISTINGUISH THE SPIN AND ORBITAL MAGNETISM

To determine the weight of spin contribution in ferromagnetism, we propose experiments involving a spin-tunneling junction consisting of Mn-doped (or Fe-doped) MoS_2 and TBG, as illustrated in Fig. 21. The transport in this junction is dependent on the spin configuration, and one can half-dope the TBG. In previous work, monolayer MoS_2 with Fe or Mn doping can be ferromagnetic with a coercivity field > 1000

Oe [86,87], while the coercivity field is ~ 200 Oe based on the measured hysteresis loops [29,38]. Thus, one can apply an external magnetic field in the range from 200 to 1000 Oe to switch the magnetic moment in TBG only. By measuring the ratio of magnetoresistance between the spin-up and spin-down channels, we can reflect the weight of spin contribution in the ferromagnetism. If the spin does not play an important role, the magnetoresistance will be vanishingly small, whereas a large magnetoresistance indicates the significance of spin. Additionally, the transport is also dependent on the orbital magnetization. In ferromagnetic MoS_2 monolayers, the valley is polarized, and one can dope one valley with a net orbital magnetic moment, as shown in Fig. 21 [70,88]. By fixing the spin as parallel in TBG and ferromagnetic MoS_2 and rotating the MoS_2 to switch the valley degree of freedom by 180°, one can determine the effect of orbital moment or Berry curvature on transport. Again, if the orbital moment is not important, the magnetoresistance will be vanishingly small, whereas a large magnetoresistance indicates the significance of orbital moment.

[1] E. Y. Andrei and A. H. MacDonald, Graphene bilayers with a twist, Nat. Mater. **19**, 1265 (2020).

[2] Y. Cao, D. Rodan-Legrain, O. Rubies-Bigorda, J. M. Park, K. Watanabe, T. Taniguchi, and P. Jarillo-Herrero, Tunable correlated states and spin-polarized phases in twisted bilayer–bilayer graphene, Nature (London) **583**, 215 (2020).

[3] M. Yankowitz, S. Chen, H. Polshyn, Y. Zhang, K. Watanabe, T. Taniguchi, D. Graf, A. F. Young, and C. R. Dean, Tuning superconductivity in twisted bilayer graphene, Science **363**, 1059 (2019).

[4] J. S. Hofmann, E. Khalaf, A. Vishwanath, E. Berg, and J. Y. Lee, Fermionic Monte Carlo study of a realistic model of twisted bilayer graphene, Phys. Rev. X **12**, 011061 (2022).

[5] Y.-X. Wang, F. Li, and Z.-Y. Zhang, Phase diagram and orbital Chern insulator in twisted double bilayer graphene, Phys. Rev. B **103**, 115201 (2021).

[6] A. Kerelsky, L. J. McGilly, D. M. Kennes, L. Xian, M. Yankowitz, S. Chen, K. Watanabe, T. Taniguchi, J. Hone, and C. Dean, Maximized electron interactions at the magic angle in twisted bilayer graphene, Nature (London) **572**, 95 (2019).

[7] B. Roy and V. Juričić, Unconventional superconductivity in nearly flat bands in twisted bilayer graphene, Phys. Rev. B **99**, 121407(R) (2019).

[8] A. T. Pierce, Y. Xie, J. M. Park, E. Khalaf, S. H. Lee, Y. Cao, D. E. Parker, P. R. Forrester, S. Chen, and K. Watanabe, Unconventional sequence of correlated Chern insulators in magic-angle twisted bilayer graphene, Nat. Phys. **17**, 1210 (2021).

[9] F. Wu and S. D. Sarma, Ferromagnetism and superconductivity in twisted double bilayer graphene, Phys. Rev. B **101**, 155149 (2020).

[10] J. Kang and O. Vafek, Strong coupling phases of partially filled twisted bilayer graphene narrow bands, Phys. Rev. Lett. **122**, 246401 (2019).

[11] Y. Saito, J. Ge, K. Watanabe, T. Taniguchi, and A. F. Young, Independent superconductors and correlated insulators in twisted bilayer graphene, Nat. Phys. **16**, 926 (2020).

[12] T. M. Wolf, O. Zilberberg, G. Blatter, and J. L. Lado, Spontaneous valley spirals in magnetically encapsulated twisted bilayer graphene, Phys. Rev. Lett. **126**, 056803 (2021).

[13] M. He, Y.-H. Zhang, Y. Li, Z. Fei, K. Watanabe, T. Taniguchi, X. Xu, and M. Yankowitz, Competing correlated states and abundant orbital magnetism in twisted monolayer-bilayer graphene, Nat. Commun. **12**, 4727 (2021).

[14] P. Stepanov, M. Xie, T. Taniguchi, K. Watanabe, X. Lu, A. H. MacDonald, B. A. Bernevig, and D. K. Efetov, Competing zero-field Chern insulators in superconducting twisted bilayer graphene, Phys. Rev. Lett. **127**, 197701 (2021).

[15] G. Wagner, Y. H. Kwan, N. Bultinck, S. H. Simon, and S. Parameswaran, Global phase diagram of the normal state of twisted bilayer graphene, Phys. Rev. Lett. **128**, 156401 (2022).

[16] M. Ochi, M. Koshino, and K. Kuroki, Possible correlated insulating states in magic-angle twisted bilayer graphene under strongly competing interactions, Phys. Rev. B **98**, 081102(R) (2018).

[17] J. M. Park, Y. Cao, K. Watanabe, T. Taniguchi, and P. Jarillo-Herrero, Tunable strongly coupled superconductivity in magic-angle twisted trilayer graphene, Nature (London) **590**, 249 (2021).

[18] A. O. Sboychakov, A. V. Rozhkov, A. L. Rakhmanov, and F. Nori, Spin density wave and electron nematicity in magic-angle twisted bilayer graphene, Phys. Rev. B **102**, 155142 (2020).

[19] M. Fidrysiak, M. Zegrodnik, and J. Spałek, Unconventional topological superconductivity and phase diagram for an effective two-orbital model as applied to twisted bilayer graphene, Phys. Rev. B **98**, 085436 (2018).

[20] H. Guo, X. Zhu, S. Feng, and R. T. Scalettar, Pairing symmetry of interacting fermions on a twisted bilayer graphene superlattice, Phys. Rev. B **97**, 235453 (2018).

[21] Y. W. Choi and H. J. Choi, Strong electron-phonon coupling, electron-hole asymmetry, and nonadiabaticity in magic-angle twisted bilayer graphene, Phys. Rev. B **98**, 241412(R) (2018).

[22] Y. Xie, A. T. Pierce, J. M. Park, D. E. Parker, E. Khalaf, P. Ledwith, Y. Cao, S. H. Lee, S. Chen, and P. R. Forrester, Fractional Chern insulators in magic-angle twisted bilayer graphene, Nature (London) **600**, 439 (2021).

[23] K. P. Nuckolls, M. Oh, D. Wong, B. Lian, K. Watanabe, T. Taniguchi, B. A. Bernevig, and A. Yazdani, Strongly correlated Chern insulators in magic-angle twisted bilayer graphene, Nature (London) **588**, 610 (2020).

[24] G. Chen, A. L. Sharpe, E. J. Fox, Y.-H. Zhang, S. Wang, L. Jiang, B. Lyu, H. Li, K. Watanabe, and T. Taniguchi, Tunable correlated Chern insulator and ferromagnetism in a moiré superlattice, Nature (London) **579**, 56 (2020).

[25] H. C. Po, L. Zou, A. Vishwanath, and T. Senthil, Origin of Mott insulating behavior and superconductivity in twisted bilayer graphene, Phys. Rev. X **8**, 031089 (2018).

[26] N. Bultinck, S. Chatterjee, and M. P. Zaletel, Mechanism for anomalous Hall ferromagnetism in twisted bilayer graphene, Phys. Rev. Lett. **124**, 166601 (2020).

[27] S. Chatterjee, N. Bultinck, and M. P. Zaletel, Symmetry breaking and skyrmionic transport in twisted bilayer graphene, Phys. Rev. B **101**, 165141 (2020).

[28] J. Cai, E. Anderson, C. Wang, X. Zhang, X. Liu, W. Holtzmann, Y. Zhang, F. Fan, T. Taniguchi, and K. Watanabe, Signatures

of fractional quantum anomalous Hall states in twisted $MoTe_2$, Nature (London) **622**, 63 (2023).
[29] A. L. Sharpe, E. J. Fox, A. W. Barnard, J. Finney, K. Watanabe, T. Taniguchi, M. Kastner, and D. Goldhaber-Gordon, Emergent ferromagnetism near three-quarters filling in twisted bilayer graphene, Science **365**, 605 (2019).
[30] J.-X. Lin, Y.-H. Zhang, E. Morissette, Z. Wang, S. Liu, D. Rhodes, K. Watanabe, T. Taniguchi, J. Hone, and J. Li, Spin-orbit–driven ferromagnetism at half moiré filling in magic-angle twisted bilayer graphene, Science **375**, 437 (2022).
[31] Y. Saito, F. Yang, J. Ge, X. Liu, T. Taniguchi, K. Watanabe, J. Li, E. Berg, and A. F. Young, Isospin Pomeranchuk effect in twisted bilayer graphene, Nature (London) **592**, 220 (2021).
[32] D. Xiao, W. Yao, and Q. Niu, Valley-contrasting physics in graphene: Magnetic moment and topological transport, Phys. Rev. Lett. **99**, 236809 (2007).
[33] J. Liu and X. Dai, Theories for the correlated insulating states and quantum anomalous Hall effect phenomena in twisted bilayer graphene, Phys. Rev. B **103**, 035427 (2021).
[34] W.-Y. He, D. Goldhaber-Gordon, and K. T. Law, Giant orbital magnetoelectric effect and current-induced magnetization switching in twisted bilayer graphene, Nat. Commun. **11**, 1650 (2020).
[35] P. Narang, C. A. Garcia, and C. Felser, The topology of electronic band structures, Nat. Mater. **20**, 293 (2021).
[36] M. Serlin, C. L. Tschirhart, H. Polshyn, Y. Zhang, J. Zhu, K. Watanabe, T. Taniguchi, L. Balents, and A. F. Young, Intrinsic quantized anomalous Hall effect in a moiré heterostructure, Science **367**, 900 (2020).
[37] K. Yoshizawa and R. Hoffmann, The role of orbital interactions in determining ferromagnetic coupling in organic molecular assemblies, J. Am. Chem. Soc. **117**, 6921 (1995).
[38] A. L. Sharpe, E. J. Fox, A. W. Barnard, J. Finney, K. Watanabe, T. Taniguchi, M. A. Kastner, and D. Goldhaber-Gordon, Evidence of orbital ferromagnetism in twisted bilayer graphene aligned to hexagonal boron nitride, Nano Lett. **21**, 4299 (2021).
[39] S.-Y. Li, Y. Zhang, Y.-N. Ren, J. Liu, X. Dai, and L. He, Experimental evidence for orbital magnetic moments generated by moiré-scale current loops in twisted bilayer graphene, Phys. Rev. B **102**, 121406(R) (2020).
[40] C. L. Tschirhart M. Serlin, H. Polshyn, A. Shragai, Z. Xia, J. Zhu, Y. Zhang, K. Watanabe, T. Taniguchi, M. E. Huber *et al.*, Imaging orbital ferromagnetism in a moiré Chern insulator, Science **372**, 1323 (2021).
[41] Y.-W. Liu, J.-B. Qiao, C. Yan, Y. Zhang, S.-Y. Li, and L. He, Magnetism near half-filling of a Van Hove singularity in twisted graphene bilayer, Phys. Rev. B **99**, 201408(R) (2019).
[42] A. Thomson, S. Chatterjee, S. Sachdev, and M. S. Scheurer, Triangular antiferromagnetism on the honeycomb lattice of twisted bilayer graphene, Phys. Rev. B **98**, 075109 (2018).
[43] L. A. Gonzalez-Arraga, J. Lado, F. Guinea, and P. San-Jose, Electrically controllable magnetism in twisted bilayer graphene, Phys. Rev. Lett. **119**, 107201 (2017).
[44] T. M. Wolf, J. L. Lado, G. Blatter, and O. Zilberberg, Electrically tunable flat bands and magnetism in twisted bilayer graphene, Phys. Rev. Lett. **123**, 096802 (2019).
[45] J. Vahedi, R. Peters, A. Missaoui, A. Honecker, and G. Trambly de Laissardière, Magnetism of magic-angle twisted bilayer graphene, SciPost Phys. **11**, 083 (2021).
[46] A. O. Sboychakov, A. V. Rozhkov, A. L. Rakhmanov, and F. Nori, Externally controlled magnetism and band gap in twisted bilayer graphene, Phys. Rev. Lett. **120**, 266402 (2018).
[47] D. V. Chichinadze, L. Classen, and A. V. Chubukov, Valley magnetism, nematicity, and density wave orders in twisted bilayer graphene, Phys. Rev. B **102**, 125120 (2020).
[48] A. Lopez-Bezanilla, Emergence of flat-band magnetism and half-metallicity in twisted bilayer graphene, Phys. Rev. Mater. **3**, 054003 (2019).
[49] D. A. Bahamon, G. Gómez-Santos, and T. Stauber, Emergent magnetic texture in driven twisted bilayer graphene, Nanoscale **12**, 15383 (2020).
[50] D. Guerci, P. Simon, and C. Mora, Moiré lattice effects on the orbital magnetic response of twisted bilayer graphene and Condon instability, Phys. Rev. B **103**, 224436 (2021).
[51] Y. Guan, O. V. Yazyev, and A. Kruchkov, Reentrant magic-angle phenomena in twisted bilayer graphene in integer magnetic fluxes, Phys. Rev. B **106**, L121115 (2022).
[52] Y. Alavirad and J. Sau, Ferromagnetism and its stability from the one-magnon spectrum in twisted bilayer graphene, Phys. Rev. B **102**, 235123 (2020).
[53] A. Fischer, L. Klebl, C. Honerkamp, and D. M. Kennes, Spin-fluctuation-induced pairing in twisted bilayer graphene, Phys. Rev. B **103**, L041103 (2021).
[54] R. Pons, A. Mielke, and T. Stauber, Flat-band ferromagnetism in twisted bilayer graphene, Phys. Rev. B **102**, 235101 (2020).
[55] F. Wu and S. D. Sarma, Collective excitations of quantum anomalous Hall ferromagnets in twisted bilayer graphene, Phys. Rev. Lett. **124**, 046403 (2020).
[56] K. Seo, V. N. Kotov, and B. Uchoa, Ferromagnetic Mott state in twisted graphene bilayers at the magic angle, Phys. Rev. Lett. **122**, 246402 (2019).
[57] E. Khalaf and A. Vishwanath, Baby skyrmions in Chern ferromagnets and topological mechanism for spin-polaron formation in twisted bilayer graphene, Nat. Commun. **13**, 6245 (2022).
[58] C. Repellin, Z. Dong, Y.-H. Zhang, and T. Senthil, Ferromagnetism in narrow bands of moiré superlattices, Phys. Rev. Lett. **124**, 187601 (2020).
[59] Y.-T. Hsu, F. Wu, and S. D. Sarma, Topological superconductivity, ferromagnetism, and valley-polarized phases in moiré systems: Renormalization group analysis for twisted double bilayer graphene, Phys. Rev. B **102**, 085103 (2020).
[60] H. X. Zhang, Y. X. Gao, and Z. J. Ding, Ferromagnetism in magic-angle twisted bilayer graphene: A Monte Carlo study, arXiv:2206.14432.
[61] T. Bömerich, L. Heinen, and A. Rosch, Skyrmion and tetarton lattices in twisted bilayer graphene, Phys. Rev. B **102**, 100408(R) (2020).
[62] C. Repellin and T. Senthil, Chern bands of twisted bilayer graphene: Fractional Chern insulators and spin phase transition, Phys. Rev. Res. **2**, 023238 (2020).
[63] P. Potasz, M. Xie, and A. H. MacDonald, Exact diagonalization for magic-angle twisted bilayer graphene, Phys. Rev. Lett. **127**, 147203 (2021).
[64] O. Vafek and J. Kang, Renormalization group study of hidden symmetry in twisted bilayer graphene with Coulomb interactions, Phys. Rev. Lett. **125**, 257602 (2020).
[65] P. M. Eugenio and C. B. Dag, DMRG study of strongly interacting $\mathbb{Z}_2$ flatbands: A toy model inspired by twisted bilayer graphene, SciPost Phys. Core **3**, 015 (2020).

[66] B. Pahlevanzadeh, P. Sahebsara, and D. Sénéchal, Charge order and antiferromagnetism in twisted bilayer graphene from the variational cluster approximation, SciPost Phys. **13**, 040 (2022).

[67] J. W. Venderbos and R. M. Fernandes, Correlations and electronic order in a two-orbital honeycomb lattice model for twisted bilayer graphene, Phys. Rev. B **98**, 245103 (2018).

[68] C.-C. Liu, L.-D. Zhang, W.-Q. Chen, and F. Yang, Chiral spin density wave and $d + id$ superconductivity in the magic-angle-twisted bilayer graphene, Phys. Rev. Lett. **121**, 217001 (2018).

[69] K. Boguslawski, C. R. Jacob, and M. Reiher, Can DFT accurately predict spin densities? Analysis of discrepancies in iron nitrosyl complexes, J. Chem. Theory Comput. **7**, 2740 (2011).

[70] Y. Lai, Z. Song, Y. Wan, M. Xue, C. Wang, Y. Ye, L. Dai, Z. Zhang, W. Yang, and H. Du, Two-dimensional ferromagnetism and driven ferroelectricity in van der Waals $CuCrP_2S_6$, Nanoscale **11**, 5163 (2019).

[71] Z. Song, Y. Wang, H. Zheng, P. Narang, and L.-W. Wang, Deep quantum-dot arrays in moiré superlattices of non-van der Waals materials, J. Am. Chem. Soc. **144**, 14657 (2022).

[72] Y. Wang, Z. Song, J. Wan, S. Betzler, Y. Xie, C. Ophus, K. C. Bustillo, P. Ercius, L.-W. Wang, and H. Zheng, Strong structural and electronic coupling in metavalent PbS moiré superlattices, J. Am. Chem. Soc. **144**, 23474 (2022).

[73] Z. Song, X. Sun, and L.-W. Wang, Eshelby-twisted three-dimensional moiré superlattices, Phys. Rev. B **103**, 245206 (2021).

[74] N. Troullier and J. L. Martins, Efficient pseudopotentials for plane-wave calculations, Phys. Rev. B **43**, 1993 (1991).

[75] S. Grimme, Semiempirical GGA-type density functional constructed with a long-range dispersion correction, J. Comput. Chem. **27**, 1787 (2006).

[76] Z. Song, X. Sun, and L. Wang, Switchable asymmetric moiré patterns with strongly localized states, J. Phys. Chem. Lett. **11**, 9224 (2020).

[77] S. Fang, S. Carr, Z. Zhu, D. Massatt, and E. Kaxiras, Angle-dependent *ab initio* low-energy Hamiltonians for a relaxed twisted bilayer graphene heterostructure, arXiv:1908.00058.

[78] S. Carr, S. Fang, Z. Zhu, and E. Kaxiras, Exact continuum model for low-energy electronic states of twisted bilayer graphene, Phys. Rev. Res. **1**, 013001 (2019).

[79] H. Tang, S. Carr, and E. Kaxiras, Geometric origins of topological insulation in twisted layered semiconductors, Phys. Rev. B **104**, 155415 (2021).

[80] A. Rozen, J. M. Park, U. Zondiner, Y. Cao, D. Rodan-Legrain, T. Taniguchi, K. Watanabe, Y. Oreg, A. Stern, and E. Berg, Entropic evidence for a Pomeranchuk effect in magic-angle graphene, Nature (London) **592**, 214 (2021).

[81] M. Angeli, E. Tosatti, and M. Fabrizio, Valley Jahn-Teller effect in twisted bilayer graphene, Phys. Rev. X **9**, 041010 (2019).

[82] J.-Y. Tsai, J. Pan, H. Lin, A. Bansil, and Q. Yan, Antisite defect qubits in monolayer transition metal dichalcogenides, Nat. Commun. **13**, 492 (2022).

[83] S. Li, G. Thiering, P. Udvarhelyi, V. Ivády, and A. Gali, Carbon defect qubit in two-dimensional WS_2, Nat. Commun. **13**, 1210 (2022).

[84] Y. Ping and T. J. Smart, Computational design of quantum defects in two-dimensional materials, Nat. Comput. Sci. **1**, 646 (2021).

[85] T. Cao, Z. Li, and S. G. Louie, Tunable magnetism and half-metallicity in hole-doped monolayer GaSe, Phys. Rev. Lett. **114**, 236602 (2015).

[86] J. Wang, F. Sun, S. Yang, Y. Li, C. Zhao, M. Xu, Y. Zhang, and H. Zeng, Robust ferromagnetism in Mn-doped Mo_2 nanostructures, Appl. Phys. Lett. **109**, 092401 (2016).

[87] K. Kang, S. Fu, K. Shayan, Y. Anthony, S. Dadras, X. Yuzan, F. Kazunori, M. Terrones, W. Zhang, and S. Strauf, The effects of substitutional Fe-doping on magnetism in MoS_2 and WS_2 monolayers, Nanotechnology **32**, 095708 (2020).

[88] Z. Song, X. Sun, J. Zheng, F. Pan, Y. Hou, M.-H. Yung, J. Yang, and J. Lu, Spontaneous valley splitting and valley pseudospin field effect transistors of monolayer $VAgP_2Se_6$, Nanoscale **10**, 13986 (2018).